Remote Sensing of Environment 113 (2009) 421–434

Contents lists available at ScienceDirect

Remote Sensing of Environment

journal homepage: www.elsevier.com/locate/rse

Detection of foliage conditions and disturbance from multi-angular high spectral resolution remote sensing

Thomas Hilker [a,*], Nicholas C. Coops [a], Samuel B. Coggins [a], Michael A. Wulder [b], Mathew Brown[c], T. Andrew Black [c], Zoran Nesic [c], Dominic Lessard [c]

[a] Faculty of Forest Resources Management, University of British Columbia, 2424 Main Mall, Vancouver, BC, V6T 1Z4, Canada
[b] Canadian Forest Service (Pacific Forestry Centre), Natural Resources Canada, 506 West Burnside Road, Victoria, BC, V8Z 1M5, Canada
[c] Faculty of Land and Food Systems, University of British Columbia, 2357 Main Mall, Vancouver, BC, V6T 1Z4, Canada

ARTICLE INFO

Article history:
Received 2 July 2008
Received in revised form 6 October 2008
Accepted 11 October 2008

Keywords:
Hyperspectral remote sensing
Multi-angular
Radiometer
AMSPEC
Disturbance
Mountain pine beetle
NDVI
Chlorophyl
Lodgepole pine
BRDF
BRF
Spectroradiometer
Canadian carbon program
Phenology
Forests

ABSTRACT

Disturbance of forest ecosystems, an important component of the terrestrial carbon cycle, has become a focus of research over recent years, as global warming is about to increase the frequency and severity of natural disturbance events. Remote sensing offers unique opportunities for detection of forest disturbance at multiple scales; however, spatially and temporally continuous mapping of non-stand replacing disturbance remains challenging. First, most high spatial resolution satellite sensors have relatively broad spectral ranges with bandwidths unsuitable for detection of subtle, stress induced, features in canopy reflectance. Second, directional and background reflectance effects, induced by the interactions between the sun-sensor geometry and the observed canopy surface, make up-scaling of empirically derived relationships between changes in spectral reflectance and vegetation conditions difficult. Using an automated tower based spectroradiometer, we analyse the interactions between canopy level reflectance and different stages of disturbance occurring in a mountain pine beetle infested lodgepole pine stand in northern interior British Columbia, Canada, during the 2007 growing season. Directional reflectance effects were modelled using a bidirectional reflectance distribution function (BRDF) acquired from high frequency multi-angular spectral observations. Key wavebands for observing changes in directionally corrected canopy spectra were identified using discriminant analysis and highly significant correlations between canopy reflectance and field measured disturbance levels were found for several broad and narrow waveband vegetation indices (for instance, $r^2_{NDVI}=0.90$; $r^2_{CHL3}=0.85$; $p<0.05$). Results indicate that multi-angular observations are useful for extraction of disturbance related changes in canopy reflectance, in particular the temporally and spectrally dense data detected changes in chlorophyll content well. This study will help guide and inform future efforts to map forest health conditions at landscape and over increasingly coarse scales.

1. Introduction

Disturbance of forest ecosystems including harvesting, fire, insect infestations, diseases, windfall, and die-back is an important component of the terrestrial carbon cycle (Houghton 1999; Kurz et al., 2008a; Masek et al., 2008; Pacala et al., 2001). Disturbance events emit carbon to the atmosphere through oxidation and decomposition of dead organic matter, while, conversely, recovery from past disturbance tends to sequester carbon from the atmosphere, often over much longer time periods (Masek et al., 2008). Study of the interactions between disturbance and carbon cycling has become of particular interest over recent years, as global warming is predicted to increase the frequency and severity of natural disturbance events (Chapin et al., 2008; Kurz et al., 2008a; Soja et al., 2007; Westerling and Bryant 2008).

Owing at least partially to favorable climatic conditions, the current epidemic of mountain pine beetle (*Dendroctonus ponderosae* Hopk.) in western Canada has reached an order of magnitude greater than any previous outbreak (Kurz et al., 2008a) with currently more than 10.1 million ha of pine forest being affected (Westfall 2007). The estimated cumulative emission of this disturbance event alone is about 270 mega-tonnes of carbon (Kurz et al., 2008a). While significance of forest disturbance for the terrestrial carbon cycle has been acknowledged in general (Kurz and Apps 1994; Kurz et al., 2008b; Margolis et al., 2006; Thornton et al., 2002), the spatio-temporal patterns of large epidemics like these remain only poorly understood (Masek et al., 2008; Pacala et al., 2001). First, insect epidemics may interact with other disturbance events in complex ways to produce multi-scale habitat diversity, from microhabitats to landscape patterns (Jogiste et al., 2007; Lerzman and Fall 1998), and second, population dynamics make accurate mapping over larger areas challenging (Aldrich 1975).

* Corresponding author. Tel.: +1 604 822 4148; fax: +1 604 822 9106.
E-mail address: thilker@interchange.ubc.ca (T. Hilker).

0034-4257/$ – see front matter © 2008 Elsevier Inc. All rights reserved.
doi:10.1016/j.rse.2008.10.003

Remote sensing offers unique opportunities to identify land cover change (Ghitter et al., 1995; Lambin and Strahler 1994) and forest disturbance in general (Collins and Woodcock 1996; Hall et al., 1991; Olsson 1994; Palmier and Ansseau 1992; Spanner et al., 1989; Wulder et al., 2004a), and various efforts have been made to map disturbance events at regional and national scales (Cayuela et al., 2006; Chastain et al., 2008; Masek et al., 2008; Sader and Legaard 2008; Wulder et al., 2004a). Most studies, however, have been focusing on stand-clearing events, such as clear-cuts or fires (Masek et al., 2008), while disturbances that leave intact substantial portions of the forest canopy, such as insect outbreaks, are much more difficult to quantify (Jin and Sader 2005; Lunetta et al., 2004; Masek and Collatz 2006; Masek et al., 2008; Wulder et al., 2005). These disturbances often cause slow die-back of individual or small clusters of trees over multiple months or years (Wulder et al., 2006) and changes in broad band canopy reflectance are only apparent as the disturbance aggregates or its magnitude increases. Difficulties in using space borne sensors to capture these more subtle changes in foliar conditions may be attributed to the relatively broad spectral and spatial ranges at which most satellite sensors operate, as the observed pixels are usually an amalgamation of disturbed and healthy tree crowns, background and shadow (Lefsky and Cohen 2003). While these limitations can be partially overcome by a higher spatial resolution which effectively reduces the number of elements contained in a pixel (Coops et al., 2006), high spatial resolution instruments generally lack the coverage required for mapping larger disturbance events.

Recently, the advent of fine spectral resolution sensors has offered new possibilities for quantifying changes in canopy conditions using narrow waveband reflectance (Ollinger et al., 2002; White et al., 2007a,b). While not yet fully operational from space, narrow waveband remote sensing holds promise to greatly enhance our capability for mapping canopy conditions as it allows to identify even subtle changes in the biochemical composition of plant foliage (Cheng et al., 2006; Curran 1989; Datt 1998; Fuentes et al., 2006; Hall et al., 2008). High spectral resolution remote sensing is therefore a potentially powerful tool for accurate mapping of vegetation conditions; extraction of physiologically relevant information, however, is not trivial (Asner 1998; Hilker et al., 2008b). For instance, investigation of stand level conditions requires consideration of the canopy structure (Gao and Schaaf 2003; Myneni et al., 1992) and this information is not easily being obtained from nadir measurements alone (Chen et al., 2003a; Strahler and Jupp 1990). Concurrent multi-angular observations can provide valuable information that characterize the structure of vegetated surfaces (Chen et al., 2003b; Gao and Schaaf 2003) at stand, local and regional scales (Hilker et al., 2008a). These multi-angular observations are, however, subject to directional and background reflectance effects (Li and Strahler 1985, 1992), which, driven by the interactions of the sun-sensor geometry and the canopy surface (Wanner et al., 1997), alter the observed reflectance of a given object, thereby confounding the desired signal used for extraction of canopy information (Hilker et al., 2008b; Los et al., 2005).

The objective of this study was to assess the potential of multi-angular, high spectral resolution remote sensing to discriminate subtle changes in foliage conditions in a mountain pine beetle infested forest stand in the northern interior part of British Columbia, Canada. Using an experimental tower-based radiometer set-up, designed to sample canopy spectra with high temporal, spatial, and spectral resolution and under multiple view and sun-angles (Hilker et al., 2007), we develop an approach to separate changes in canopy reflectance induced by bark beetle disturbance from directional and background reflectance effects (Hilker et al., 2008b; Los et al., 2005). Key wavebands are identified using stepwise forward and normal discriminant analysis and compared to field observations. Our findings have significant implications for future research as they demonstrate a potential way to accurately map foliage conditions and vegetation disturbance using airborne or spaceborne sensors.

2. Methods

2.1. Research site

The focus of this study is an 80-100-year-old, 15-m tall lodgepole pine (*Pinus contorta* Dougl. ex. Loud var. *latifolia* Engl.) stand near Mackenzie, British Columbia, Canada (55.111944° N, 122.839722° W; Elevation: 740 m above sea level). The forest stand is part of the sub-boreal spruce bio-geoclimatic zone and receives an annual average precipitation of about 655 mm. The stand structure is open and has a basal area of about 60 m^2 ha^{-1} and an average stocking density of about 1500 stems per ha. The understorey is sparse and consists of various mosses and a few low shrubs and pine seedlings. The site was initially infested by mountain pine beetle in August 2006. A second attack following in the summer of 2007 resulted in an additional infestation of the study area. Fig. 1A–C shows a series of photographs of the stand taken at the beginning of the experiment (April 25) and during two field assessments made in June and October 2007, respectively. The canopy was still largely green in late April with most of the attacked trees turning red during late May through early June and a continued decline of the health status of the canopy through to October.

2.2. Mountain pine beetle

Lodgepole pine (*Pinus contorta* Dougl. ex. Loud var. *latifolia* Engl.) is the primary host of mountain pine beetle in British Columbia. The beetle typically emerges in late July/early August. Once a suitable host is found, large numbers of beetles may overwhelm the defences of a given host and proceed to bore through the bark, burrow horizontal galleries, laying eggs as they excavate. When the eggs hatch, the larvae begin to feed around the stem perpendicular to the main gallery, also a fungus inoculated into the phloem and sapwood by attacking beetles

Fig. 1. Photographs of the research site taken on April 25 (A), June 26 (B) and October 17 (C). The canopy was still largely green in late April with most of the attacked trees turning red during late May through early June. The health status of the canopy declined further through to October and more foliage turned red.

provides nutrients to feeding larvae. The combination of gallery construction and the growth of fungal hyphae clog the phloem leading to limited translocation and eventually halt the transport of nutrients from roots to foliage. As a result, the foliage of a successfully mass-attacked tree will fade from green through shades of yellow to red, finally to be shed once sufficiently dry (see Wulder et al., 2006 for details on the link between foliar fading and remote detection). The change in foliage color typically occurs at the beginning of the next vegetation period (spring of the year following the attack), as the nutrient transport is cut off shortly before the attacked trees go dormant over the winter period. Typically, foliage fades over a period of 12 months, but can begin to fade shortly after attack, fading is more obvious in the proceeding spring and summer, so that foliage on trees attacked in the previous year appears red (Carroll and Safranyik 2003). The time period between the attack and the change of color in the foliage is referred to in here as green attack stage, which is followed by the red attack stage, defined as the time period after which the foliage has faded to red as a result of the attack (Fig. 2). Gray attack describes the final stage at which the tree has no needles left, usually after 2–3 years (Wulder et al., 2006).

2.3. Acquisition of remote sensing data

Canopy spectra were observed from an automated multi-angular spectroradiometer platform (AMSPEC), mounted at a height of 30.5 m on a 1.5 m×2.1 m (5′×7′) scaffold tower (Fig. 2A, B) which has been installed at the site as part of the Canadian Carbon Program to measure the CO_2 fluxes using the eddy covariance technique. AMSPEC was designed for high-frequency observations of canopy reflectance (Hilker et al., 2007). The instrument features a motor-driven probe that allows observations in a 290° view area around the tower (the 70° that cannot be observed are due to obstruction by the tower). The probe rotates in 11.5° intervals every 30 s, completing a full rotation every 15 min. The exact position of the probe is determined using a potentiometer attached to the shaft of the motor. At the end of each sweep, the sensor is returned to its original position. The spectroradiometer used is a Unispec-DC (PP Systems, Amesbury, MA, USA) featuring 256 contiguous bands with a nominal band spacing of 3 nm and a nominal range of operation between 350 and 1200 nm (Hilker et al., 2007). To allow sampling under varying sky conditions, canopy reflectance is obtained from simultaneous measurements of solar irradiance and radiance, sampled every 5 s from sunrise to sunset. The upward looking probe is equipped with a cosine receptor (PP-Systems) to correct sky irradiance measurements for varying solar altitudes. The downward looking probe measures canopy radiance at a zenith angle of 62° to account for canopy clumping (Chen and Black 1991) and to minimize background reflectance effects. The probe's instantaneous field of view (IFOV) is 20°, or approximately 33×7 m at canopy height. The instrument's footprint results from its setup geometry and comprises an outer diameter of about 116 m while the inner diameter is about 46 m. A complete technical description of the instrument its software, setup and calibration can be found in Hilker et al. (2007). The instrument was installed on April 25 at the site and spectra were sampled continuously through October 17, 2007.

2.4. Filtering data acquired under sunny sky conditions

AMSPEC data were filtered for clear sky observations to eliminate expected changes in canopy reflectance as a function of cloudiness (Hilker et al., 2008b) and also because it was anticipated that optimal results for the modeling of BRDF would be achieved under clear sky conditions with directional reflectance effects being predominant (Hilker et al., 2008b). Furthermore, clear sky conditions show a more representative subset of data when comparing these measurements to airborne or spaceborne data. Sky conditions for each sampled spectrum were identified by modeling clear sky solar irradiance as a function of the solar azimuth using a 2nd degree polynomial function derived from a subset of radiometer irradiance observations obtained for 4 completely clear days, selected in approximately evenly distributed intervals throughout the observation period. Measured solar irradiance from the radiometer was then compared to modelled clear sky solar radiation and spectral observations were rejected when their irradiance component deviated by more than a given threshold (5%) from the modelled clear sky irradiance.

2.5. Field based assessment of canopy conditions

Field data were collected on June 26, 2007 within a ring-shaped plot around the flux-tower, defined using the inner and outer diameter of AMSPEC's set-up geometry. The health status of each tree within the plot was determined by visually assessing the canopy condition and searching the bark for boreholes. Each tree was then classified into one of four classes: “healthy” (if the canopy was green and no boreholes were found), “green attacked” (if the canopy was green, but boreholes were found), “red attacked” (if the canopy was red), or “without needles”. AMSPEC observes reflectance as aggregate of all tree crowns lying within a radiometer observed view area (segment). Consequently, the health conditions of trees observed within the plot had to be aggregated to make them comparable to radiometer observed reflectance values. Using a differentially

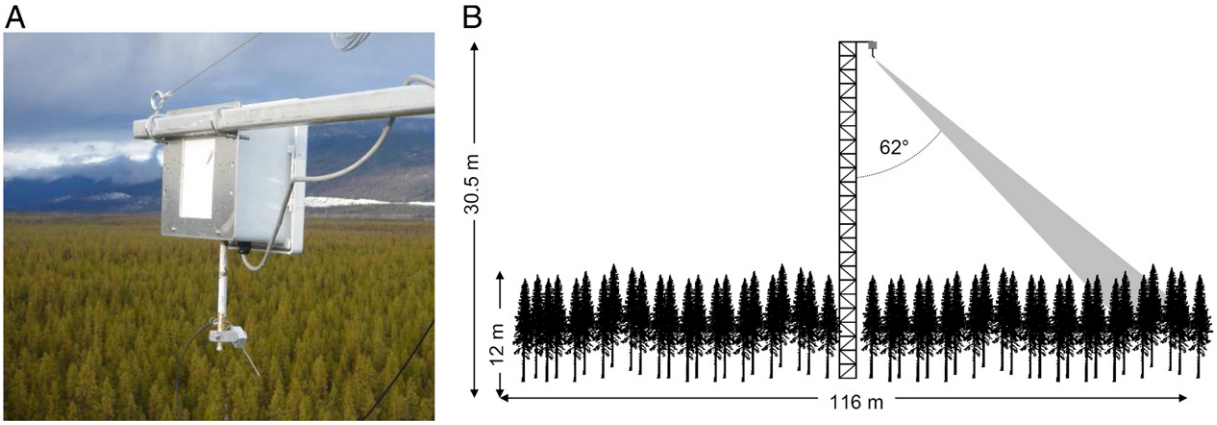

Fig. 2. A: Photograph of the tower mounted radiometer platform (AMSPEC) used to observed canopy reflectance changes due to mountain pine beetle attack. B: Setup and footprint of AMSPEC. The footprint observed varies slightly with individual tree height and differences in terrain height. The vertical zenith angle is 62°, the approximate footprint size is 116 m (diameter), the instrument is installed about 18 m above the canopy. The 70° area located in the radiometer's blind spot on the south side of the tower was excluded from the analysis.

corrected GPS (Ranger Pro XT, Trimble, Sunnyvale, California), the plot was first subdivided into 23° segments, each of which covered the approximate view area of two probe positions of AMSPEC (23° segments were chosen to make the field measurements more spatially representative). A coded value was then assigned to each tree according to its field assessed class (code for "healthy" = 2, "green attacked" = 3, "red attacked" = 4, "without needles" = 5) and the average disturbance per segment was calculated using the arithmetic mean of the health conditions assigned to the individual trees within a segment. Since the GPS measured corner locations of each segment are only an approximation of the radiometer observed field of view, the overlapping area fractions between field observed segments and radiometer observed segments were determined in a post-processing step and the health status of the field data was linearly interpolated using these overlapping area fractions to spatially match the radiometer observations.

The progression of the mountain pine beetle attack throughout the vegetation period was determined from re-assessing the health status of each individual tree on October 17, 2007 to represent the status after the second attack during late summer 2007. The aggregated health status per segment was compared in the described way. Additionally, the health status for April (before the trees faded from green to yellow to red) was predicted from June data, making the assumption that all red attacked trees observed in June were at the green attack stage in April, as during the installation of AMSPEC no red tree crowns had been observed.

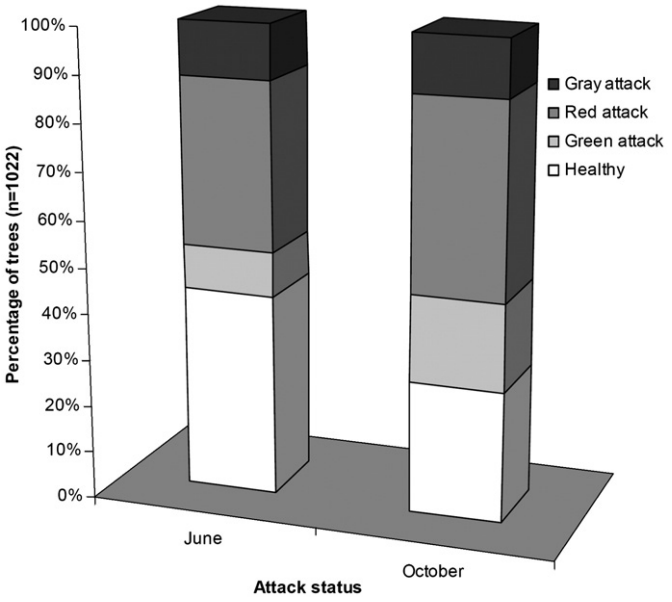

Fig. 4. Health status observed by field measurements on June 28 and October 17. The health status of each tree was assessed visually and trees were classified as either healthy (code = 2), green attacked (code = 3), red attacked (code = 4) or gray attack (= without needles) (code = 5).

2.6. Isolating disturbance related changes in spectra using BRDF

Optical remote sensing is governed by shadowing and scatterer-specular reflectance effects (Privette et al., 1996), which results in spectral observations appearing brighter or darker as a result of the interaction of solar irradiance with a given surface and sun-observer geometry (Roujean et al., 1992). One possible way to model directional reflectance effects is using a BRDF, which describes how land surface reflectance varies with view zenith, solar zenith and azimuth angle (Barnsley and Kay 1990; Gao and Schaaf 2003; Wanner et al., 1995a). Among the most commonly applied BRDF models is the semi-empirical kernel driven representation (Roujean et al., 1992), which describes BRDF as a linear superposition of a set of basic BRDF shapes based on relative sun position and simple measures of the canopy structure (Wanner et al., 1995a). The common application is related to simplicity of model specification that allows acquisition of model parameters from mathematical inversion of relatively few multi-angular reflectance observations, thereby facilitating applications over a wide range of spatial scales. A series of different mathematical kernels can be selected to optimize BRDF models for various kinds of vegetation cover. In temperate climatic zones and when observing discontinuous, stacked canopies (e.g., conifer stands), the bidirectional reflectance distribution is most commonly represented by the so called the Li-Sparse (LS) and Ross-Thick (RT) kernels (Wanner et al., 1995b), based on a geometric-optical approach (Li and Strahler 1985) and the radiative transfer theory (Ross 1981):

$$\rho(\theta_v, \theta_s, \Delta\phi) = k_i + k_g K_L\left(\theta_v, \theta_s, \Delta\phi, \frac{h}{b}, \frac{b}{r}\right) + k_v, K_R(\theta_v, \theta_s, \Delta\phi) \quad (1)$$

where k_i, k_g and k_v are the isotropic, geometric and volumetric scattering components and K_L and K_R are the Li-Sparse and Ross-Thick kernels, respectively. θ_v, θ_s and Δ represent view zenith, solar zenith and the relative azimuth angle between the sun and the observer, whereas $\frac{h}{b}$ and $\frac{b}{r}$ describe crown relative height and crown relative shape, in here defined as constant values of 1 and 2, respectively (Wanner et al., 1995a). ρ describes the reflectance of a given wavelength.

While the Li-Sparse and Ross-Thick kernels can be used to assess directional reflectance under the assumption of homogenous surfaces,

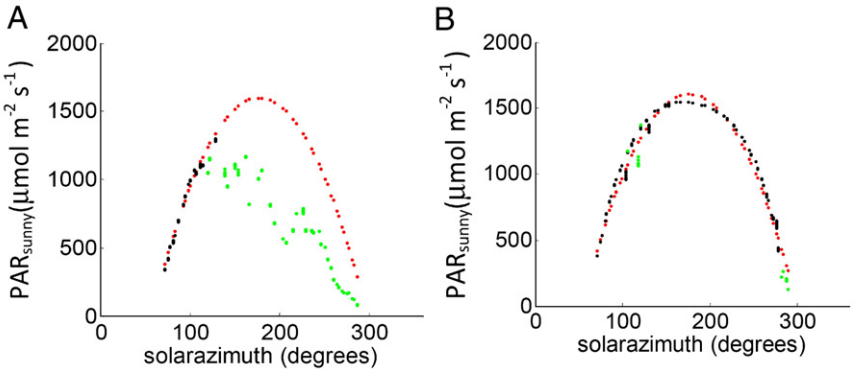

Fig. 3. Example of the clear sky filtering algorithm for two given days. The red dots show the modeled clear sky PAR values, the black dots the observed and accepted radiometer observations, the green dots show the observed and rejected radiometer observations. DOY 137 was a clear day until about 10 a.m. (A), whereas DOY 144 was mostly clear throughout (B).

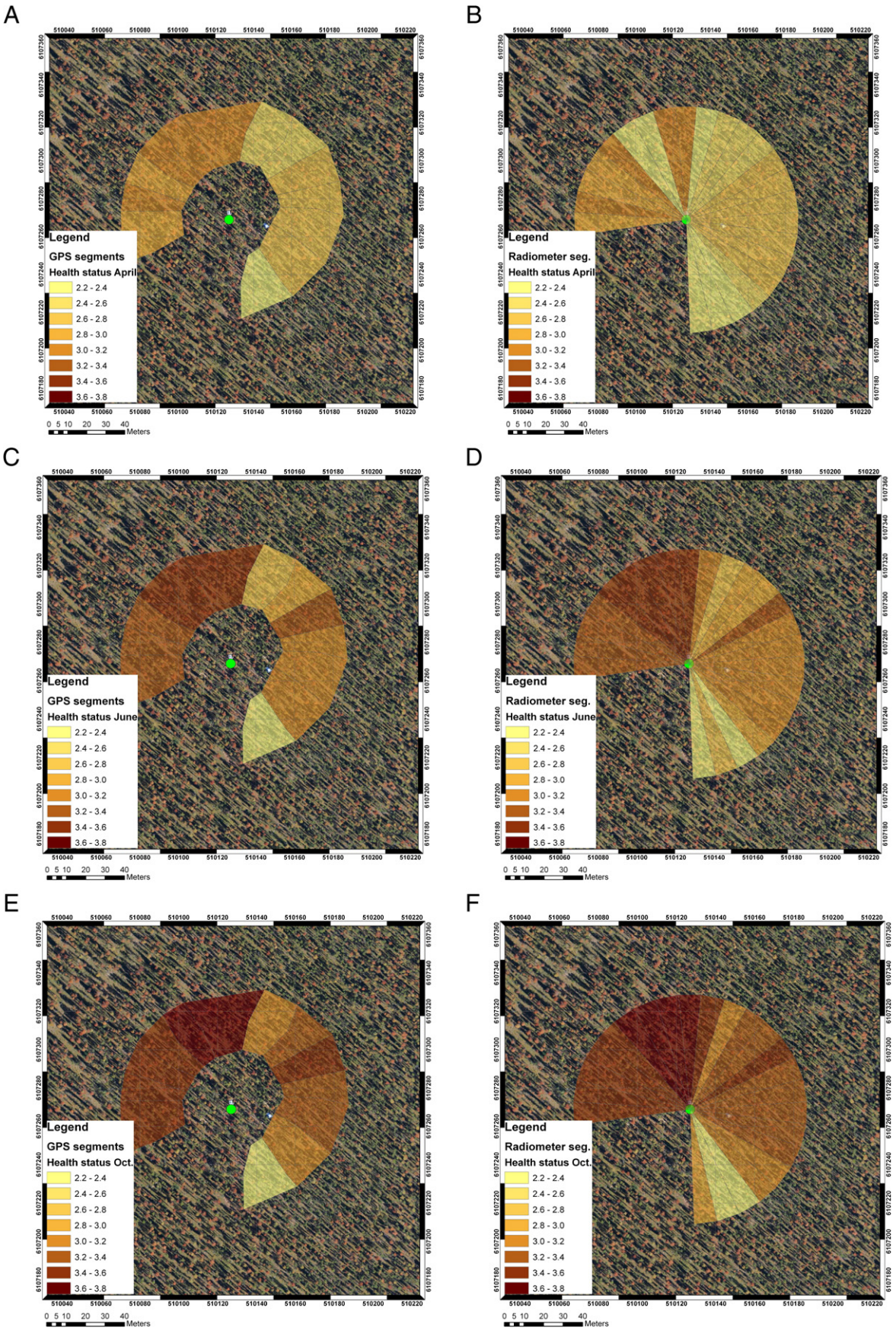

Fig. 5. Segment aggregated health status as determined by field measurements for GPS measured segments (left column, A,C, and E) and radiometer observed segments (right column, B,D, and F) for the month of April, June and October, respectively. The health status shown for the radiometer segments (Fig. 5 B, D and F) was used as a basis to stratify the spectral observations into the eight different levels with separate BRDF models being computed for each strata and 14 day interval.

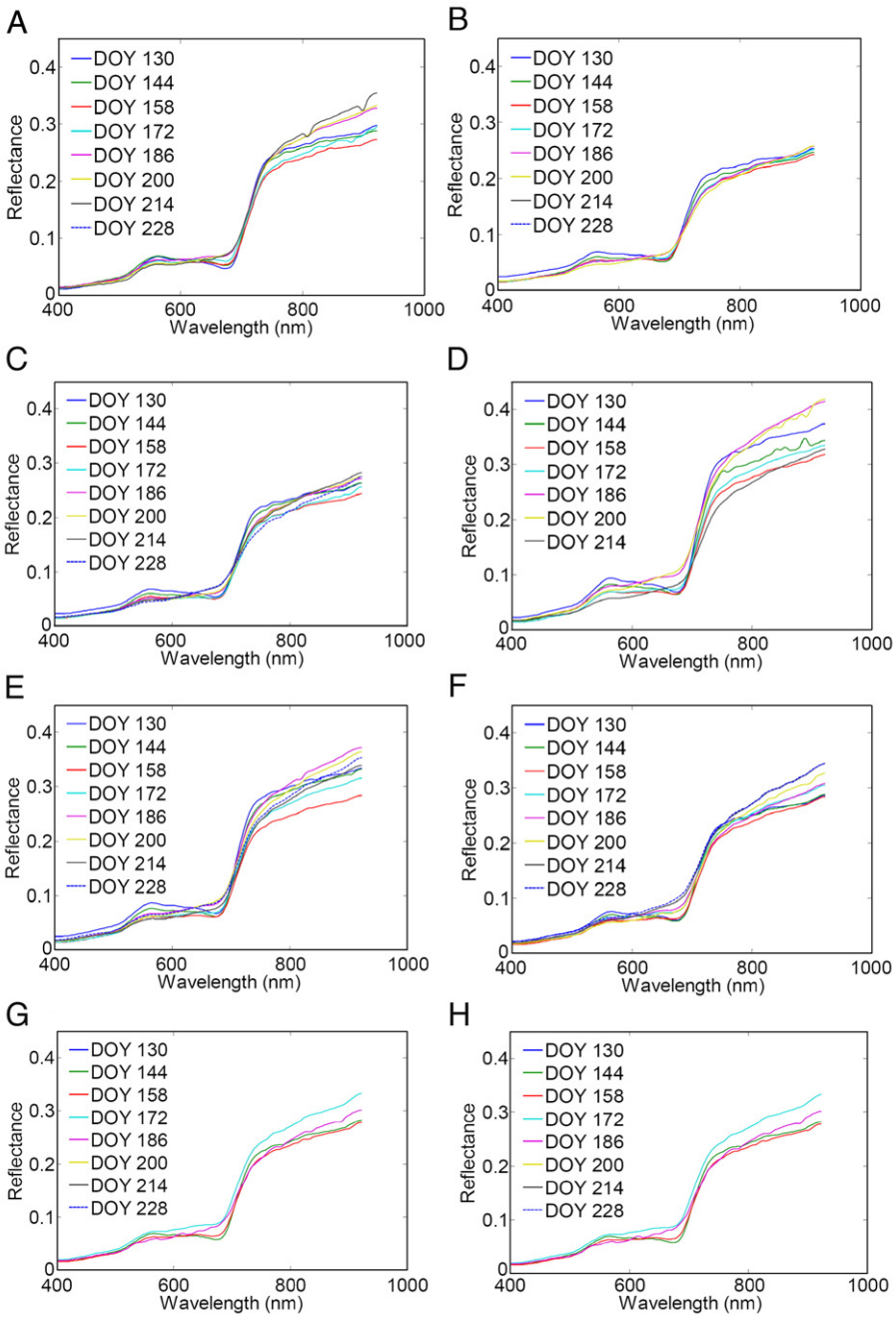

Fig. 6. A–H: Time series of BRDF corrected surface reflectance for the eight infestation levels (A–H) shown in Fig. 5 between DOY 130 and DOY 228. Reflectances derived from inverse and forward modeling of the BRDF using the stratified spectra as inputs. The result is one standardized spectrum per strata and time interval. (No BRDF corrected spectrum is shown in panel D for DOY 228 as for this specific canopy location and time period there were not enough clear sky observations with sufficient variability in the sun-observer geometry to derive a stable BRDF model from mathematical inversion).

reflectance values observed by AMSPEC were expected to vary not only as a function of BRDF, but also because of spatial and temporal differences in disturbance intensity observed over time. Hilker et al. (2008b) demonstrated that observations of heterogeneous surfaces can be isolated from BRDF effects (Strahler and Jupp 1990) when stratifying spectra into homogeneous subsets of observations with respect to the changing surface condition (in this case foliage conditions are changing over space and time) and subsequently fitting individual BRDF models to each of these strata.

In the spatial domain, field-based assessment of disturbance was used to stratify the canopy segments into eight different strata within which the spectral variation related to forest disturbance was expected to be negligible. In the temporal domain, separate BDRF models were fitted to spectral observations in 14-day time intervals, since the progressing disturbance was expected to change the canopy reflectance over time.

Once a BRDF model is established from a series of multi-directional measurements, reflectance can be estimated for any possible sun-observer geometry (Hilker et al., 2008b; Wanner et al., 1995a), thereby allowing direct inter-comparison of multi-angular observations. This is accomplished by normalizing reflectance measurements to one common sun observer geometry (in this case sun position was selected to be that at the summer solstice, with the observing probe looking north), which results in one modeled and representative reflectance value per stratum and time interval (Hilker et al., 2008b). Since scattering and directional reflectance effects will vary with wavelengths, separate BRDF models also need to be derived for each waveband under investigation. In this study we

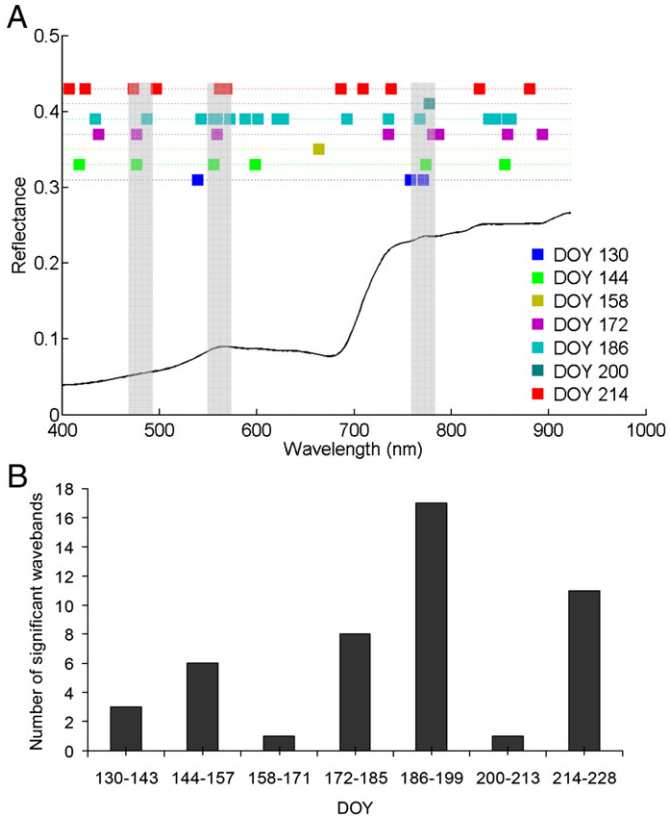

Fig. 7. A: Location of the most significant wavebands for identifying disturbance levels in 14-day intervals as identified by stepwise forward and normal discriminant analysis. Spectral separability of disturbance levels for the marked wavebands was significant at an a-level of 0.05 with $p<0.001$, using Wilks' Lambda test. The squares identify the location of the waveband within the electromagnetic spectrum, the colors correspond to the different 14-day intervals. The grey bars highlight waveband regions for which disturbance levels where significantly separable for four or more 14 day periods. B: Number of wavebands that showed a significant spectral separability of disturbance levels over time. The time period with most the wavebands suitable for detection of foliage conditions was around DOY 186.

conducted a full spectral analysis of all 3-nm wavebands between 400 and 950 nm and compared them to the different levels of infestation over time.

2.7. Identifying key wavebands using discriminant analysis

Key wavebands for determination of foliage conditions over time were identified from BRDF-corrected spectra using stepwise forward and normal discriminant analysis. Daily BRDF models were established and spectra were normalized and grouped according to the field observed infestation levels in 14-day time steps. Spectra were smoothed using a Gaussian filter function and the curve shape of each spectrum was determined using its first numerically derived derivative (van Aardt and Wynne 2001). To decrease the number of independent spectral wavebands, a stepwise discriminant procedure was applied first, based on the definitions of van Aardt and Wynne (2001). This procedure was followed by a normal discriminant analysis to identify those bands that showed the highest separability with respect to field-measured disturbance levels and the accuracy of the normal discriminant analysis was assessed using a cross-validation approach (van Aardt and Wynne 2001).

2.8. Assessing canopy health status from spectral vegetation indices

Based on the results of the discriminant analysis, a number of narrow and broader band vegetation indices were identified and tested for their ability to distinguish different levels of mountain pine beetle infestation at the research site. Vegetation indices were selected so that the detection band of each index falls approximately within the spectral zones found to be significantly related to

Table 1
Description of vegetation indices used for determination of mountain pine beetle infestation, their primary absorption feature and reference source.

Index name	Definition	Related wavebands	Major application	References
Normalized difference vegetation index *NDVI*	$=\frac{\rho_{NIR}-\rho_{Red}}{\rho_{NIR}+\rho_{Red}}$	ρ_{NIR} = mean ρ between 800-900 nm wavelength. ρ_{Red} = mean ρ between 600-670 nm wavelength	Detection of vegetation greenness.	(Myneni and Williams, 1994; Sellers, 1985; Tucker, 1979)
Chlorophyll 1 index CHL_1	$=\frac{\frac{1}{\rho_{green}}-\frac{1}{\rho_{NIR}}}{\frac{1}{\rho_{green}}+\frac{1}{\rho_{NIR}}}$	ρ_{green} = mean ρ between 525-555 nm wavelength.	Detection of chlorophyll contents	(Gitelson et al., 2003)
Chlorophyll 2 index CHL_2	$=\frac{\frac{1}{\rho_{595-725}}-\frac{1}{\rho_{NIR}}}{\frac{1}{\rho_{595-725}}+\frac{1}{\rho_{NIR}}}$	$\rho_{595-725}$ = mean ρ between 595-725 nm wavelength.	Detection of chlorophyll contents	(Gitelson et al., 2003)
Chlorophyll 3 index CHL_3	$=\frac{P_{694}-P_{760}}{P_{694}+P_{760}}$	P_{694} = mean ρ between 694-760 nm wavelength ρ_{760} = mean ρ between 694-760 nm wavelength	Used for detection of vegetation stress	(Carter and Miller, 1994)
Ratio vegetation index RVI	$=\frac{\rho_{800}-\rho_{680}}{\rho_{800}+\rho_{680}}$	$\rho_{800}=\rho$ at 800 nm wavelength $\rho_{680}=\rho$ at 680 nm wavelength	Detection of vegetation stress and chlorophyll.	(Pearson and Miller, 1972)
Red green index RGI	$=\frac{P_{green}-P_{red}}{P_{red}+P_{green}}$	ρ_{green} = mean ρ between 540-600 nm ρ_{red} mean ρ between 600-670 nm	Detection of mountain pine beetle red attack	(Coops et al., 2006)

mountain-pine-beetle-induced disturbance levels by the discriminant analysis.

Computation of directionally-corrected spectral vegetation indices, such as a normalized-difference reflectance of two wavebands, can be achieved by correcting both directionally-corrected wavelengths separately before computing the normalized difference. A BRDF of a spectral vegetation index (SVI) can, however, also be obtained for a normalized-difference index by applying a mathematical inversion directly (Hilker et al., 2008b; Los et al., 2005). This approach has the advantage that the residual errors are directly minimized with respect to the index observed (Los et al., 2005).

3. Results

Fig. 3 shows an example of the filtering technique applied to identify clear sky situations by comparing the radiometer measured photosynthetically active radiation with modelled clear sky irradiance on a daily basis. For day of year (DOY) 137, as shown in Fig. 3A, skies were clear until about 10 AM, measurements after this time were rejected due to increasing cloudiness, evident by the reduction in measured sky irradiance. For the second example, almost all measurements were accepted as DOY 144 was a completely clear day (Fig. 3B).

A total of 1022 trees were found within the radiometer footprint (Fig. 2B). In June, about 43% of these trees were healthy, 10% were in a green attack state, 36% were red attacked and 11% had no foliage on them. The re-assessment of the disturbance conditions in October yielded a 25% decrease in healthy trees (total healthy trees: 28%), 19% of the trees were green-attacked while 41% were in a red-attack state (Fig. 4). Fig. 5 shows the spatial distribution of mountain pine beetle infestation assessed from field data observed in June (C and D) and October (E and F) 2007 and predictions made for April (A and B). The figures in the left column (A,C,E) represent the infestation rates per GPS measured field segment, the figures on the right (B,D, and F) show the field measured infestation rates transferred to the radiometer observed field of view. The colors in the figure correspond to 8 different levels of infestation. Using field observations, disturbance was found to be highest in the area north of the tower with most of the trees being either at the red attack stage or without needles; whereas, infestation rates were lowest in the south east.

The change of the BRDF corrected spectra between 400 and 950 nm wavelengths over time and for the different infestation classes observed is shown in Fig. 6. Fig. 6A–H correspond to the eight different infestation levels from the least infested (6A) to the most severely damaged stratum (6H). The most apparent change in spectra considering all strata is the decrease in green and near infrared reflectance over time (Curran et al.,

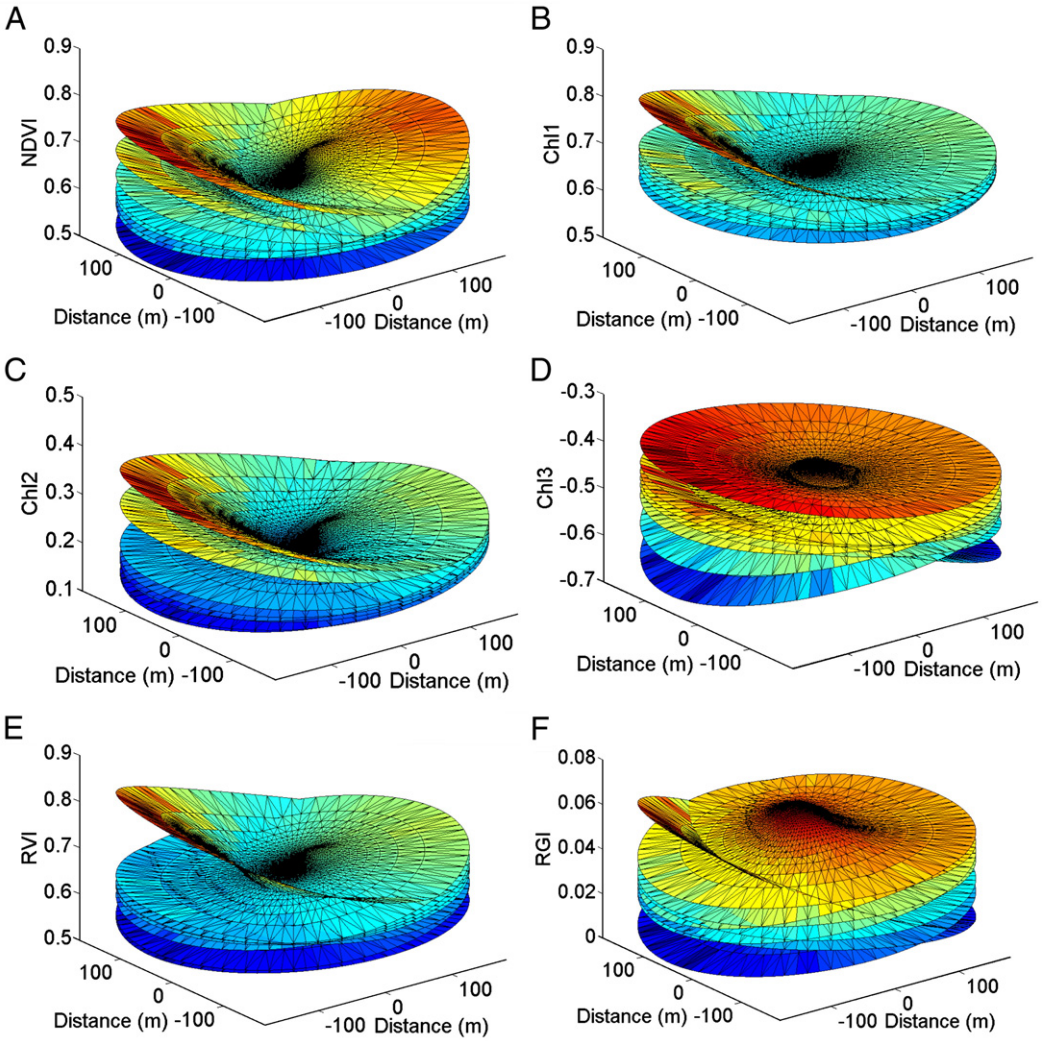

Fig. 8. A–F: BRDF surfaces determined for the examined vegetation indices (A) NDVI, (B) CHL1, (C) CHL2, (D) CHL3, (E) RVI (F)RGI for the example of DOY 144–158. Each surface shown within a subfigure represents a different infestation class (bottom = least damaged, top = most damaged). The *x* and *y* axis is showing the distance in meters from the tower (center), the *z*-axis is showing the corresponding index-value.

1991; Horler et al., 1983; Miller et al., 1991) which is evident especially at the higher levels of infestation. Additionally, the reflectance in the green band decreases over time over all infestation levels as the foliage turns from green to yellow to red with changes in reflectance being visible on a 14-day basis. No clear sky observations were made after DOY 228.

The spectral regions suitable for detection of foliage conditions varied over time, however, the wavebands at approximately 490 nm, 560 nm, and 780 nm seemed most suitable for discriminating the difference disturbance throughout the observation period (Fig. 7a). The squares identify the location of the most significant wavebands within the electromagnetic spectrum; the colors correspond to the 14-day intervals. Spectral regions that showed the highest degree of discrimination with respect to field measured disturbance conditions over time are highlighted in grey. Fig. 7B shows the variation of the number of spectral bands suitable for detection of foliage conditions induced by mountain pine beetle infestation with the examined 14-day intervals. Generally, the number of significant wavebands for discriminating foliage conditions was higher towards the end of the vegetation period when changes in canopy appearance were more apparent. The number of wavebands for discriminating foliage conditions was largest for the 14-day time period near DOY 186 but was significantly reduced during the transition period from green to red attack in early June (DOY 158) as well as during the second mountain pine beetle attack period in late July (DOY 200) (Fig. 7B).

Table 1 shows an overview of the spectral vegetation indices selected for description of mountain pine beetle induced disturbance levels. Fig. 8A–F shows a stack of BRDF models derived for these vegetation indices using a single 14-day interval as an example (DOY 144–158). Each BRDF surface represents the modelled reflectance of a specific health stratum as determined from field-based observations. The *x*- and *y*-axis show the distance (in m) from the tower, the *z*-axis shows the reflectance values for each SVI; the colors are used to emphasize the changes in observed reflectance with the view angle. While the radiometer observes spectra at a fixed radius around the tower, BRDF can be used to model reflectance values for any off-nadir direction. For most of the indices shown in Fig. 8, the BRDF surfaces are clearly distinct from each other as a result of field observed differences in disturbance.

Fig. 9A to F shows the relationship between the BRDF corrected SVIs and field measured disturbance for the example of one 14-day period (DOY 144–158, corresponding to Fig. 8). Each sub-figure represents one SVI (as indicated in the figure captions), each data point per sub-figure represents the BRDF-normalized reflectance value for a given health stratum. During the time period shown in this example, most of the indices examined in this study were able to describe spatial changes in canopy health conditions well, with best results found for NDVI and CHL_3, respectively (r^2=0.90 and 0.87 for NDVI and CHL_3, respectively (p<0.05)).

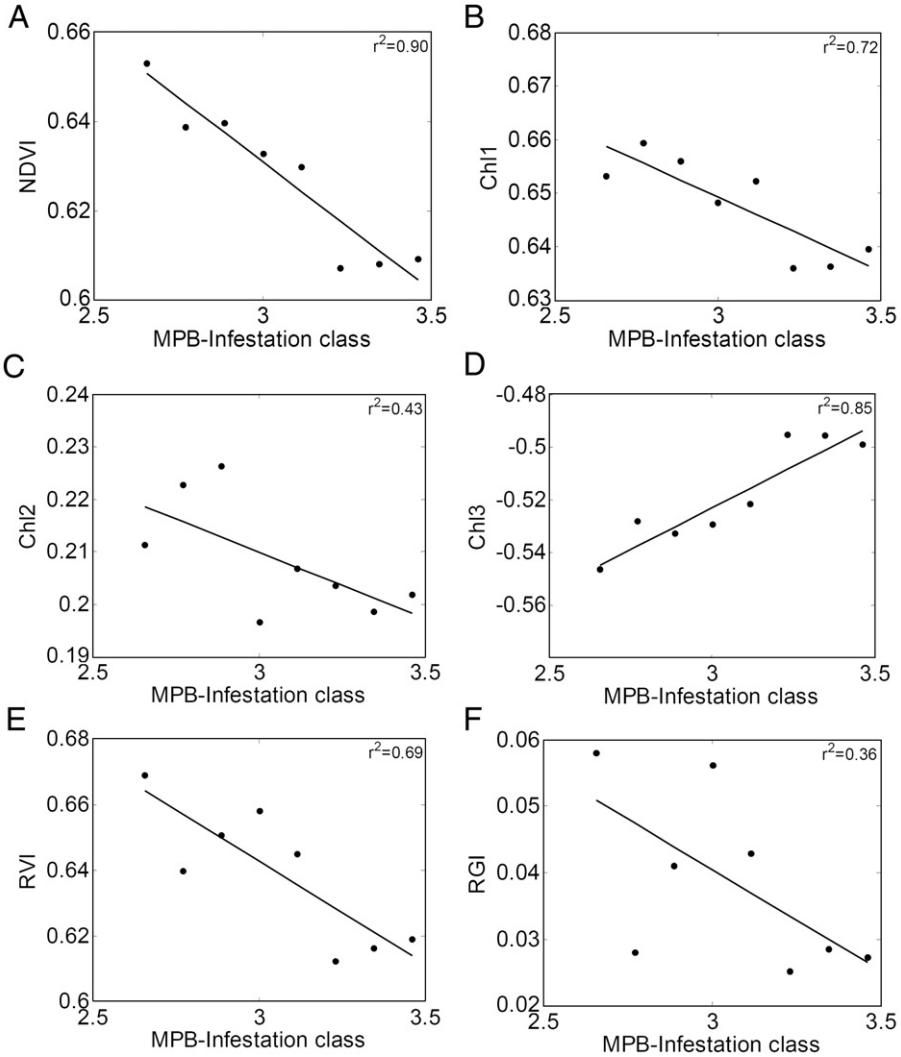

Fig. 9. A–F: Relationship between BRDF corrected vegetation indices (A) NDVI, (B) CHL1, (C) CHL2, (D) CHL3, (E) RVI (F)RGI and field observed mountain pine beetle infestation levels for the example of DOY 144–158 (p for all indices<0.05). Note that slope of the CHL3 index differs in its tendency from the other indices as a result of its definition (the index is negative).

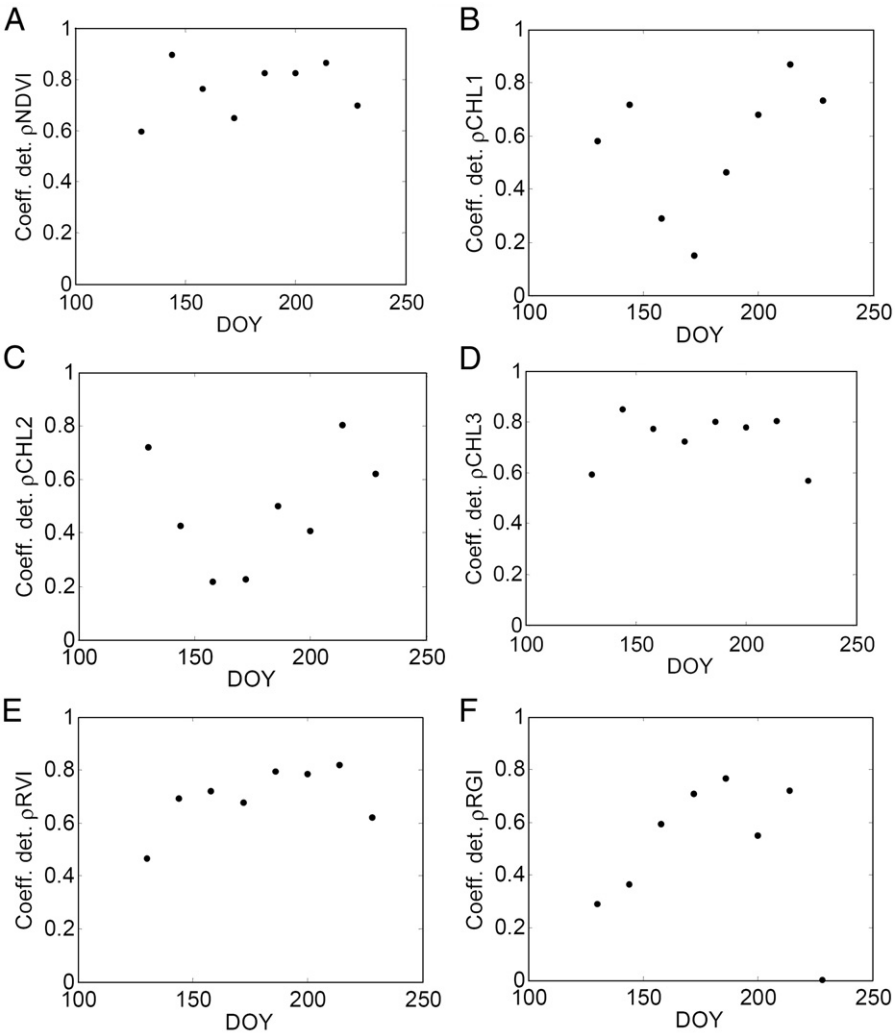

Fig. 10. A–F: Time series of the coefficient of determination observed for the relationship between different BDRF corrected reflectance indices and field observed infestation levels at DOY 130 and 228 (The coefficients of determination shown for 144–158 correspond to the values shown in Fig. 9; $p<0.05$) .

The coefficients of determination for the relationship between the BRDF corrected SVIs and field-observed infestation levels (corresponding to Fig. 9) are presented in Fig. 10A–F for all 14-day intervals between DOY 114 to DOY 228. The relationship is based on the simplifying assumption that the relative health status of the segments with respect to each other stays approximately constant between April to May, June to mid July and then through to October, based on the attack cycle of the mountain pine beetle (Carroll and Safranyik 2003 and Wulder et al., 2006). As a result, disturbance observations made in June 2006 were assumed to be representative of all 14 day periods between DOY 144 and 199, the assessments made in April and October were assumed to be representative of all 14-day intervals before and after this period, respectively. The disturbance-related differences between the individual segments were best described by NDVI and CHL_3 throughout the entire vegetation period, with high coefficients of determination found even for those 14-day intervals during which the stand was still in a green attack stage with no apparent visible changes in leaf color (see Fig. 1A). The RGI used in previous studies to detect mountain pine beetle infestation (Coops et al., 2006), as well as the RVI, showed low performance during the beginning of the vegetation period, with only a minor ability to distinguish between different levels of green attack, but showed significantly enhanced abilities after the needles turned red during mid to late-May. The chlorophyll-sensitive CHL_1 and CHL_2 indices were able to distinguish the different levels of infestation well in the beginning and the end of the growing season with lower performance shown between DOY 144 and DOY 200.

Fig. 11 shows the slope of the relationship between the BRDF corrected SVIs and field-observed infestation levels (corresponding to Fig. 9) for all 14-day intervals between DOY 114 to DOY 228. Significant and consistent changes in slope through time were found for all indices with decreasing slopes in the positive indices (NDVI, CHL_1, CHL_2, RGI, RVI) and increasing slopes from 0.04 to 0.17 in the negative index (CHL_3) as the foliage faded from green to yellow to red and then into the second green attack stage beginning in August 2007 (DOY 200–214).

4. Discussion

This study investigated the interactions between canopy reflectance and disturbance-induced changes in foliage conditions for a mountain pine beetle infested lodgepole pine stand in northern British Columbia, Canada. The field observations taken in June and October yielded a high spatial variability of levels of infestation around the tower, with overall levels of disturbance increasing from April to June to October. Averaging the coded health status of the individual trees within each segment was a simple yet successful method to describe the health status of the field observed segments. It has to be noted, however, that a change from green to red is unable to be

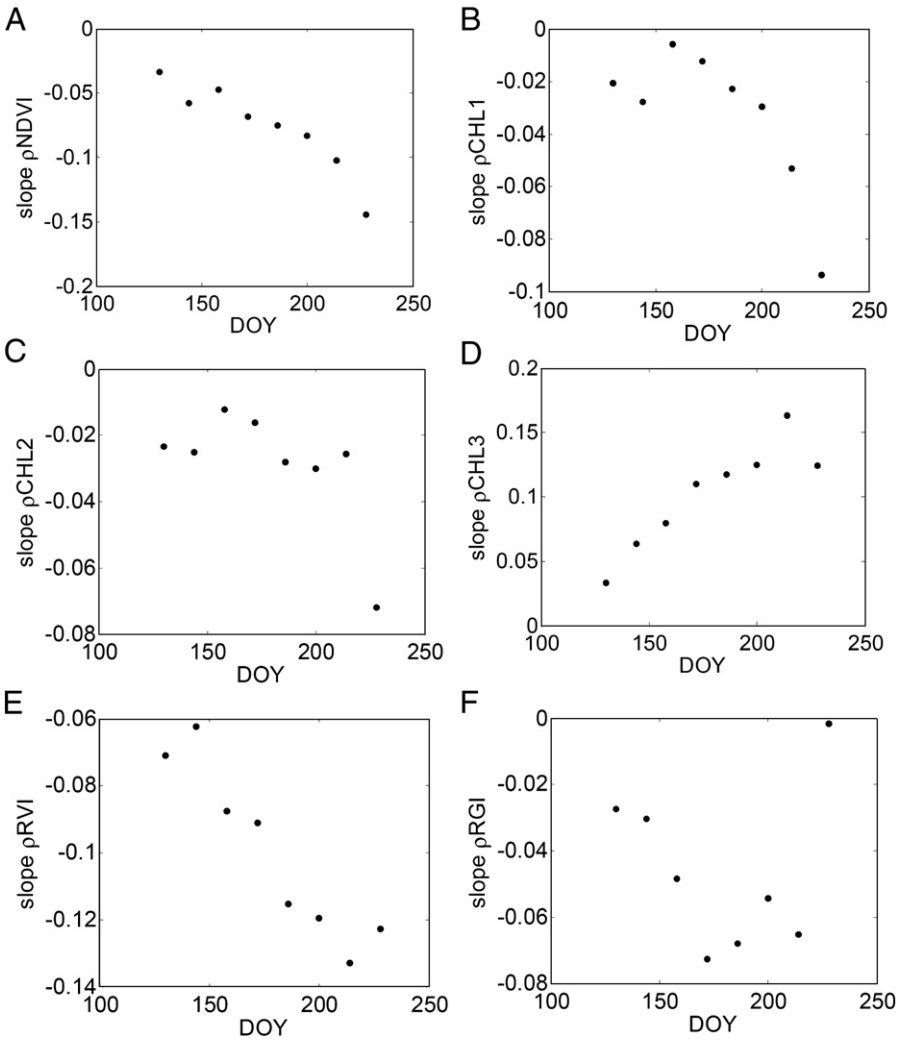

Fig. 11. A–F: Development of the slope of the relationship between different BDRF corrected reflectance indices and field observed infestation levels at DOY 130 and 228. The slope of the relationship between field observations and reflectance signal is expected to change gradually over time as the health status of the trees is declining (The slopes shown for the different indices for DOY 144–158 correspond to the slopes seen in Fig. 9).

differentiated from a change from red to gray and as a result, the method is limited to situations where no or only little changes in gray attack are occurring over the observation period (Fig. 7). Additionally, this simple method yields no absolute measure of disturbance, but only provides a means by which the disturbance found in different radiometer observed segments can be quantified with respect to each other.

Clear sky observations were effectively identified by comparing measured solar irradiance to a simple polynomial model, thereby eliminating changes in spectral reflectance due to different states of cloudiness (Hilker et al., 2008b). Stratification of these clear sky observations with respect to disturbance and fitting different BRDF models to each stratum was a successful approach for separating directional and disturbance related changes in canopy level reflectance thereby confirming findings of previous studies (Hilker et al., 2008b; Los et al., 2005). This is an important result as it underlines the capability of this approach to apply bi-directional reflectance distribution models to various kinds of heterogeneous canopy surfaces, whether they originate from different disturbance levels or other sources such as mixed species composition or physiological states (Hilker et al., 2008b). The Ross-Thick and Li-Sparse kernels (Roujean et al., 1992) were successfully used to normalize stratified observations to a common sun-observer geometry, thereby facilitating a direct comparison between observations taken in different directions from the tower and over different 14-day intervals throughout the vegetation period of 2007. The results shown in Fig. 6 and 7 demonstrate the capacity of multi-angular observations for predicting changes in canopy health, with differences in reflectance being visible as the foliage of the infested trees faded from green to yellow to red. As opposed to previous studies using broader band satellite observations (Coops et al., 2006; Wulder et al., 2004b; Wulder et al., 2006), multi-angular radiometer observations were not only able to identify both red and green attack, but it was also possible to quantify subtle differences in disturbance levels using spectral reflectance. The results shown in Fig. 7 also give an explanation why broader bands in the green and near infrared region were most successful in determining mountain pine beetle red attack, since they contain most of the significant wavebands identified using discriminant analysis. Changes in canopy reflectance over time were most apparent at the higher levels of infestation (Figs. 6E–H, 7B), for which the foliage appearance also underwent the most dramatic changes. Fig. 7A demonstrated that the disturbance-sensitive wavebands vary with the time interval observed, which could be explained by the different attack stages (green attack, red attack and second attack in August 2007, around DOY 200) the foliage underwent throughout the vegetation period. Despite this variation however, Fig. 7 confirmed that the green and near infrared regions were most suitable for detection of mountain pine beetle induced disturbance over time, with the highest number of bands found in the near infrared region. The results shown in Fig. 7B have important

implications for the selection of the time period chosen for observation of mountain pine beetle disturbance with remote sensing instruments, as a notable variation was found in the number of wavebands suitable for detection of disturbance levels over time. As a result, not all wavebands are useful for detection of pine beetle disturbance throughout the entire observation periods, and the indices used for detection of disturbance need to be adapted to the stage of disturbance. Especially during the transition periods from green- to red-attack and the new green attack, fewer wavebands were able to distinguish between foliage conditions, while the results shown in Fig. 7B suggest that the time period between early- to mid-July is most suitable for detecting mountain pine beetle induced disturbance, especially when using broader band satellite instruments.

Discriminant analysis successfully identified wavebands that were able to distinguish disturbance-induced changes in canopy reflectance at a statistically significant level ($p<0.05$). The results of the discriminant analysis were confirmed by the results shown in Figs. 10 and 11. It can be seen from Fig. 10 that most of the multi-angular vegetation indices, even when sampled over broader spectral ranges (Fig. 10a), were able to clearly detect subtle changes in disturbance levels when comparing the reflectance values of the different segments around the tower. This important result underlines the increased potential of multi-angular observations for detecting changes in canopy reflectance compared to nadir looking instruments. These results also confirm findings of previous studies undertaken in different contexts (Chen et al., 2003a; Chen et al., 2005; Goel and Grier 1988; Hilker et al., 2008b; Strahler and Jupp 1990).

Figs. 10 and 11 reveal that especially the multi-angular NDVI and CHL_3 indices were able to predict infestation levels from canopy reflectance not only during the summer periods when changes reflectance were readily apparent, but also when the infested trees were still at the green attack stage. The coefficient of determination between field and reflectance observed disturbance was >0.6 for NDVI and CHL_3 throughout the observation period and, additionally, changes in slope of reflectance observed between different segments over time shows that the progression in disturbance is being reflected in the spectral observations. The fact that even the broad band multi-angular NDVI showed high correlations to the field-observed health status throughout the year is encouraging, as it suggests that subtle changes in forest health may be observable from currently available broader band multi-angular satellite sensors such as the multi-angle imaging spectroradiometer (MISR) on board NASA's EOS-1 spacecraft TERRA. Confounding issues related to signal-to-noise, spatial resolution, and atmospheric conditions, among others, are expected challenges for utilization of space-borne instrumentation for detection of mountain pine beetle infestation conditions (see White et al., 2007a,b). The RGI, which was successfully used in previous studies (Coops et al., 2006) for mapping mountain pine beetle red attack showed good correlations to field observations only after the majority of attacked trees turned red and changes in canopy reflectance became readily apparent. This result is consistent with Fig. 7, which suggests that changes in canopy spectra were first visible in the near infrared and a few narrow wavebands in the green region of the spectrum. While this study has shown the limitation of the RGI, which largely fails to predict mountain pine beetle disturbance during its earlier phases, the high coefficients of determination found during the second half of the vegetation period underlines the potential of the RGI for measuring more severe disturbance levels, thereby confirming the findings of previous studies (Coops et al., 2006).

The slopes of the regressions between the BRDF corrected SVIs and field-observed infestation (Fig. 11) revealed a consistent decrease for the positive vegetation indices (NDVI, CHL_1, CHL_2, RGI, RVI) and a consistent increase for the CHL_3 over the period of observation. This result is expected as the health condition of the segments observed by the radiometer is constantly declining thereby leading to more dramatic changes in spectral variation over time. These findings also underline the results shown in Fig. 10 confirming the potential of the examined vegetation indices to predict disturbance at the study site.

The off-nadir viewing direction helped mitigating background reflectance effects by looking at stacks of multiple canopies. Further research will be required to examine the impact of background and other reflectance altering considerations such as atmospheric effects and fine-scale changes in the landscape pattern. This study provided an analysis of spectral reflectance properties at a canopy scales; however, additional research will be required to confirm the findings of this study over larger areas and at the landscape level. For instance, the empirically derived relationships between the field-observed disturbance levels and spectral vegetation indices are likely to change with species composition and stand properties such as nutrient and water supply.

Extensive field work was required to allow stratification of the observed canopy surface into homogenous areas, which may limit the applicability of this study over larger areas. This issue could possibly overcome by defining representative (non-infested) training areas for which the BRDF is known. Multi-angular observations of a similar, but infested stands can then be used to determine the level of infestation from applying this BRDF to the data and looking remaining difference in reflectance observed at multiple view angles (similar to Fig. 11).

The study area for which this multi-angular technique has been demonstrated is relatively small and, as a result, the findings of this research can not easily be generalized across the landscape. For instance, further research will be required to investigate the impact of species composition, understory and stand structure on broad scaled multi-angular observations. As a result, the findings of this study are more of theoretical nature and were intended to show the potential of high resolution, multi-angular observations for the determination of fine scale changes in canopy disturbance. Our findings can help guiding the application of spectral vegetation indices for determining canopy disturbance at different stages and will also have possible implications for the design of future airborne observations or satellite missions.

While the approach introduced in this study is in its current form not practically applicable over large areas, our results have demonstrated the potentials of multi-angular narrow waveband observations to continuously detect and quantify subtle changes in canopy stresses and non-stand replacing disturbance events. Future satellite sensors can help overcome some of the technical limitations inherent to this approach in its current form, thereby helping to facilitate accurate mapping of landscape level vegetation disturbance from space with potential implications for forest management, forest health monitoring and development of mitigation strategies. The technique introduced in this study has further demonstrated that the challenge of temporally continuous mapping of canopy disturbance can be overcome when separating physiologically and directionally induced changes in canopy reflectance for instance using a simple stratification approach. The results found in this study therefore underline the usefulness of multi-angular remote sensing for assessing subtle changes in foliage conditions and demonstrate their potential for characterizing subtle changes in disturbance.

5. Conclusions

- Multi-angular observations of canopy reflectance are a powerful tool for quantifying subtle changes in canopy health conditions, such as originating from bark beetle induced disturbance events.
- Disturbance induced changes in canopy reflectance of heterogeneous stands can be isolated from other effects by stratifying multi-angular spectra into homogeneous subsets of observations and subsequently fitting BRDF models to each stratum.
- The most disturbance-sensitive wavebands in this study varied with the stage of mountain pine beetle attack, and as a result, not all spectral vegetation indices were useful for year round determination of

mountain pine beetle disturbance. Best results were achieved using multi-angular observations of NDVI and CHL_3 indices.
- The period between early- to mid-July was found to be most suitable for detecting mountain pine beetle induced disturbance events, as during this time the largest number of disturbance sensitive wavebands has been identified.

Acknowledgements

We would like to thank UBC Soil Physics and Biometeorology Group (Faculty of Land and Food Systems) technicians, Rick Ketler, Andrew Sauter and Andrew Hum for assistance in the technical design, installation, and maintenance of the radiometer platform. Danny Grills (Natural Resources Canada, Canadian Forest Service) and Rory Tooke (UBC) are thanked for field assistance. This project was funded by the Government of Canada through the Mountain Pine Beetle Initiative, a six-year, $40 million program administered by Natural Resources Canada, Canadian Forest Service. Additional information on the Mountain Pine Beetle Initiative may be found at: http://mpb.cfs.nrcan.gc.ca/.

References

Aldrich, R. (1975). Detecting disturbances in a forest environment. *Photogrammetric Engineering & Remote Sensing*, *41*, 39–48.

Asner, G. (1998). Biophysical and biochemical sources of variability in canopy reflectance. *Remote Sensing of Environment*, 64.

Barnsley, M., & Kay, S. (1990). The relationship between sensor geometry, vegetation-canopy geometry and image variance. *International Journal of REmote Sensing*, *11*, 1075–1083.

Carroll, A., & Safranyik, L. (2003). The bionomics of the mountain pine beetle in lodgepole pine forests: Establishing a context. In T. Shore, J. Brooks, & J. Stone (Eds.), *Victoria, British Columbia: Natural Resources Canada, Canadian Forest Service, Pacific Forestry Centre* (pp. 21–32).

Carter, G. A., & Miller, R. L. (1994). Early detection of plant stress by digital imaging within narrow stress-sensitive wavebands. *Remote Sensing of Environment*, *50*, 295–302.

Cayuela, L., Golicher, D. J., & Rey-Benayas, J. M. (2006). The extent, distribution, and fragmentation of vanishing Montane cloud forest in the Highlands of Chiapas, Mexico. *Biotropica*, *38*, 544–554.

Chapin, F. S., Trainor, S. F., Huntington, O., Lovecraft, A. L., Zavaleta, E., Natcher, D. C., McGuire, A. D., Nelson, J. L., Ray, L., Calef, M., Fresco, N., Huntington, H., Rupp, T. S., Dewilde, L., & Naylor, R. L. (2008). Increasing wildfire in Alaska's boreal forest: Pathways to potential solutions of a wicked problem. *BioScience*, *58*, 531–540.

Chastain, R. A., Struckhoff, M. A., He, H. S., & Larsen, D. R. (2008). Mapping vegetation communities using statistical data fusion in the Ozark National Scenic Riverways, Missouri, USA. *Photogrammetric Engineering and Remote Sensing*, *74*, 247–264.

Chen, J., & Black, T. (1991). Measuring leaf area index of plant canopies with branch architecture. *Agricultural and Forest Meteorology*, *57*, 1–12.

Chen, J. M., Liu, J., Leblanc, S. G., Lacaze, R., & Roujean, J. L. (2003). Multi-angular optical remote sensing for assessing vegetation structure and carbon absorption. *Remote Sensing of Environment*, *84*, 516–525.

Chen, J. M., Liu, J., Leblanc, S. G., Lacaze, R., & Roujean, J. L. (2003). Multi-angular optical remote sensing for assessing vegetation structure and carbon absorption. *Remote Sensing of Environment*, *84*, 516–525.

Chen, J. M., Menges, C. H., & Leblanc, S. G. (2005). Global mapping of foliage clumping index using multi-angular satellite data. *Remote Sensing of Environment*, *97*, 447–457.

Cheng, Y. F., Gamon, J. A., Fuentes, D. A., Mao, Z. Y., Sims, D. A., Qiu, H. L., Claudio, H., Huete, A., & Rahman, A. F. (2006). A multi-scale analysis of dynamic optical signals in a Southern California chaparral ecosystem: A comparison of field, AVIRIS and MODIS data. *Remote Sensing of Environment*, *103*, 369–378.

Collins, J. B., & Woodcock, C. E. (1996). An assessment of several linear change detection techniques for mapping forest mortality using multitemporal landsat TM data. *Remote Sensing of Environment*, *56*, 66–77.

Coops, N. C., Johnson, M., Wulder, M. A., & White, J. C. (2006). Assessment of QuickBird high spatial resolution imagery to detect red attack damage due to mountain pine beetle infestation. *Remote Sensing of Environment*, *103*, 67–80.

Curran, P. (1989). Remote sensing of foliar chemistry. *Remote Sensing of Environment*, *30*, 271–278.

Curran, P., Dungan, B., Macler, B., & Plummer, S. (1991). The effect of a red leaf pigment on the relationship between red edge and chlorophyll concentration. *Remote Sensing of Environment*, *35*, 69–76.

Datt, B. (1998). Remote sensing of chlorophyll a, chlorophyll B, chlorophyll a+B, and total carotenoid content in Eucalyptus leaves. *Remote Sensing of Environment*, *66*, 111–121.

Fuentes, D. A., Gamon, J. A., Cheng, Y. F., Claudio, H. C., Qiu, H. L., Mao, Z. Y., Sims, D. A., Rahman, A. F., Oechel, W., & Luo, H. Y. (2006). Mapping carbon and water vapor fluxes in a chaparral ecosystem using vegetation indices derived from AVIRIS. *Remote Sensing of Environment*, *103*, 312–323.

Gao, W., & Schaaf, C. B. (2003). *Detecting vegetation structure using a kernel-based BRDF model* (pp. 86).

Ghitter, G. S., Hall, R. J., & Franklin, S. E. (1995). Variability of Landsat Thematic Mapper Data in boreal deciduous and mixed-wood stands with conifer understory. *International Journal of REmote Sensing*, *16*, 2989–3002.

Gitelson, A. A., Gritz, Y., & Merzlyak, M. N. (2003). Relationships between leaf chlorophyll content and spectral reflectance and algorithms for non-destructive chlorophyll assessment in higher plant leaves. *Journal of Plant Physiology*, *160*, 271–282.

Goel, N. S., & Grier, T. (1988). Estimation of canopy parameters for inhomogeneous vegetation canopies from reflectance data 3. Trim-a model for radiative-transfer in heterogeneous 3-dimensional canopies. *Remote Sensing of Environment*, *25*, 255–293.

Hall, F. G., Botkin, D. B., Strebel, D. E., Woods, K. D., & Goetz, S. J. (1991). Large-scale patterns of forest succession as determined by remote-sensing. *Ecology*, *72*, 628–640.

Hall, F. G., Hilker, T., Coops, N. C., Lyapustin, A., Huemmrich, F., Middleton, E., Margolis, H., Drolet, G., & Black, T. (2008). Multi-angle remote sensing of forest light use efficiency by observing PRI variation with canopy shadow fraction. *Remote Sensing of Environment*, *112*, 3201–3211.

Hilker, T., Coops, N. C., Hall, F. G., Black, T. A., Chen, B., Krishnan, P., Wulder, M. A., Sellers, P. J., Middleton, E. M., & Huemmrich, K. F. (2008). A modeling approach for up-scaling gross ecosystem production to the landscape scale using remote sensing data. *Journal of Geophysical Research–Biogeosciences*, *113*, G03006.

Hilker, T., Coops, N. C., Hall, F. G., Black, T. A., Wulder, M. A., Nesic, Z., & Krishnan, P. (2008). Separating physiologically and directionally induced changes in PRI using BRDF models. *Remote Sensing of Environment*, *112*, 2777–2788.

Hilker, T., Coops, N. C., Nesic, Z., Wulder, M. A., & Black, A. T. (2007). Instrumentation and approach for unattended year round tower based measurements of spectral reflectance. *Computers and Electronics in Agriculture*, *56*, 72–84.

Horler, D. N. H., Dockray, M., & Barber, J. (1983). The red edge of plant leaf reflectance. *International Journal of REmote Sensing*, *4*, 273–288.

Houghton, R. A. (1999). The annual net flux of carbon to the atmosphere from changes in land use 1850–1990. *Tellus Series B-Chemical and Physical Meteorology*, *51*, 298–313.

Jin, S., & Sader, S. (2005). Comparison of time series tasseled cap wetness and the normalized difference moisture index in detecting forest disturbances. *Remote Sensing of Environment*, *94*, 364–372.

Jogiste, K., Kuuluvainen, T., & Kangur, A. (2007). Disturbances at multiple scales as the basis of forest ecosystem restoration and management — Introduction. *Forest Ecology and Management*, *250*, 1–2.

Kurz, W., & Apps, M. (1994). The carbon budget of Canadian forests: A sensitivity analysis of changes in disturbance regimes, growth rates, and decomposition rates. *Environmental Pollution*, *83*, 55–61.

Kurz, W. A., Dymond, C. C., Stinson, G., Rampley, G. J., Neilson, E. T., Carroll, A. L., Ebata, T., & Safranyik, L. (2008). Mountain pine beetle and forest carbon feedback to climate change. *Nature*, *452*, 987–990.

Kurz, W. A., Stinson, G., Rampley, G. J., Dymond, C. C., & Neilson, E. T. (2008). Risk of natural disturbances makes future contribution of Canada's forests to the global carbon cycle highly uncertain. *Proceedings of the National Academy of Sciences of the United States of America*, *105*, 1551–1555.

Lambin, E. F., & Strahler, A. H. (1994). Change-vector analysis in multitemporal space–a tool to detect and categorize land–cover change processes using high temporal-resolution satellite data. *Remote Sensing of Environment*, *48*, 231–244.

Lefsky, M., & Cohen, F. (Eds.) (2003). Selection of remotely sensed data. *Remote sensing of forest environments:Concepts and case studies*.

Lerzman, A., & Fall, A. (1998). From forest stands to landscapes: spatial scales and the roles of disturbance. In D. L. Peterson & V. T. Parker (Eds.), *Ecological scale: Theory and applications* (pp. 339–367). : Columbia University Press (1998).

Li, X., & Strahler, A. (1985). Geometric-optical modeling of a conifer forest canopy. *IEEE Transactions on Geoscience and Remote Sensing*, *GE-23*, 705–721.

Li, X., & Strahler, A. (1992). Geometric-optical bidirectional reflectance modeling of the discrete crown vegetation canopy: Effect of crown shape and mutual shadowing. *IEEE Transactions on Geoscience and Remote Sensing*, *30*, 276–292.

Los, S. O., North, P. R. J., Grey, W. M. F., & Barnsley, M. J. (2005). A method to convert Avhrr normalized difference vegetation index time series to a standard viewing and illumination geometry. *Remote Sensing of Environment*, *99*, 400–411.

Lunetta, R. S., Johnson, D. M., Lyon, J. G., & Crotwell, J. (2004). Impacts of imagery temporal frequency on land-cover change detection monitoring. *Remote Sensing of Environment*, *89*, 444–454.

Margolis, H. A., Flanagan, L. B., & Amiro, B. D. (2006). The Fluxnet-Canada Research Network: Influence of climate and disturbance on carbon cycling in forests and peatlands. *Agricultural and Forest Meteorology*, *140*, 1–5.

Masek, J. G., & Collatz, G. J. (2006). Estimating forest carbon fluxes in a disturbed southeastern landscape: Integration of remote sensing, forest inventory, and biogeochemical modeling. *Journal of Geophysical Research-Biogeosciences*, *111*.

Masek, J. G., Huang, C. Q., Wolfe, R., Cohen, W., Hall, F., Kutler, J., & Nelson, P. (2008). North American forest disturbance mapped from a decadal Landsat record. *Remote Sensing of Environment*, *112*, 2914–2926.

Miller, J., Wu, J., Boyer, M., Belanger, M., & Hare, E. (1991). Seasonal patterns in leaf reflectance red-edge characteristics. *International Journal of REmote Sensing*, *12*, 1509–1523.

Myneni, R., & Williams, D. (1994). On the relationship between FAPAR and NDVI. *Remote Sensing of Environment*, *49*, 200–211.

Myneni, R. B., Asrar, G., & Hall, F. G. (1992). A 3-dimensional radiative-transfer method for optical remote-sensing of vegetated land surfaces. *Remote Sensing of Environment*, *41*, 105–121.

Ollinger, S. V., Smith, M. L., Martin, M. E., Hallett, R. A., Goodale, C. L., & Aber, J. D. (2002). Regional variation in foliar chemistry and N cycling among forests of diverse history and composition. *Ecology*, *83*, 339–355.

Olsson, H. (1994). Changes in satellite-measured reflectances caused by thinning cuttings in boreal forest. *Remote Sensing of Environment*, *50*, 221–230.

Pacala, S. W., Hurtt, G. C., Baker, D., Peylin, P., Houghton, R. A., Birdsey, R. A., Heath, L., Sundquist, E. T., Stallard, R. F., Ciais, P., Moorcroft, P., Caspersen, J. P., Shevliakova, E., Moore, B., Kohlmaier, G., Holland, E., Gloor, M., Harmon, M. E., Fan, S. M., Sarmiento, J. L., Goodale, C. L., Schimel, D., & Field, C. B. (2001). Consistent land- and atmosphere-based US carbon sink estimates. *Science*, *292*, 2316–2320.

Palmier, C., & Ansseau, C. (1992). *Remote sensing of physiological disturbances related to sugar maple dieback in southern Quebec: Potentials of imaging spectrometry.*

Pearson, L., & Miller, L. D. (1972). Remote mapping of standing crop biomass for estimation of the productivity of the short-grass prairie, pawnee national grasslands. *In 8th International Symposium on Remote Sensing of the Environment* (pp. 1357–1381). Colorado.

Privette, J. L., Emery, W. J., & Schimel, D. S. (1996). Inversion of a vegetation reflectance model with Noaa Avhrr data. *Remote Sensing of Environment*, *58*, 187–200.

Ross, J. K. (1981). *The radiation regime and architecture of plant stands.* : The Hague: Dr. W. Junk Publishers.

Roujean, J. L., Leroy, M., & Deschamps, P. Y. (1992). A bidirectional reflectance model of the earth's surface for the correction of remote-sensing data. *Journal of Geophysical Research-Atmospheres*, *97*, 20455–20468.

Sader, S. A., & Legaard, K. R. (2008). Inclusion of forest harvest legacies, forest type, and regeneration spatial patterns in updated forest maps: A comparison of mapping results. *Forest Ecology and Management*, *255*, 3846–3856.

Sellers, P. (1985). Canopy reflectance, photosynthesis and transpiration. *International Journal of Remote Sensing*, *6*, 1335–1372.

Soja, A. J., Tchebakova, N. M., French, N. H. F., Flannigan, M. D., Shugart, H. H., Stocks, B. J., Sukhinin, A. I., Varfenova, E. I., Chapin, F. S., & Stackhouse, P. W. (2007). Climate-induced boreal forest change: Predictions versus current observations. *Global and Planetary Change*, *56*, 274–296.

Spanner, M., Hlavka, C., & Pierce, L. (1989). *Analysis of forest disturbance using TM and AVHRR data* (pp. 1387–1390).

Strahler, A., & Jupp, D. (1990). Modelling bidirectional reflectance of forests and woodlands using boolean models and geometric optics. *Remote Sensing of Environment*, *34*, 153–166.

Thornton, P. E., Law, B. E., Gholz, H. L., Clark, K. L., Falge, E., Ellsworth, D. S., Golstein, A. H., Monson, R. K., Hollinger, D., Falk, M., Chen, J., & Sparks, J. P. (2002). Modeling and measuring the effects of disturbance history and climate on carbon and water budgets in evergreen needleleaf forests. *Agricultural and Forest Meteorology*, *113*, 185–222.

Tucker, C. (1979). Red and photographic infrared linear combinations for monitoring vegetation. *Remote Sensing of Environment*, *8*, 127–150.

van Aardt, J. A. N., & Wynne, R. H. (2001). Spectral separability among six southern tree species. *Photogrammetric Engineering and Remote Sensing*, *67*, 1367–1375.

Wanner, W., Li, X., & Strahler, A. (1995). On the derivation of kernels for kernel-driven models of bidirectional reflectance. *Journal of Geophysical Research*, *100*, 21 077–021 089.

Wanner, W., Li, X., & Strahler, A. H. (1995). On the derivation of kernels for kernel-driven models of bidirectional reflectance. *Journal of Geophysical Research-Atmospheres*, *100*, 21077–21089.

Wanner, W., Strahler, A., Hu, B., Lewis, P., Muller, J., Li, X., Barker Schaaf, C., & Barnsley, M. (1997). Global retrieval of bidirectional reflectance and albedo over land from EOS MODIS and MISR data: Theory and algorithm. *Journal of Geophysical Research*, *102*, 17 143–117 161.

Westerling, A. L., & Bryant, B. P. (2008). Climate change and wildfire in California. *Climatic Change*, *87*, S231–S249.

Westfall, J. (2007). *Summary of forest health conditions in British Columbia.* Victoria: British Columbia Ministry of Forests and Range.

White, J. C., Coops, N. C., Hilker, T., Wulder, M. A., & Carroll, A. L. (2007). Detecting mountain pine beetle red attack damage with Eo-1 hyperion moisture indices. *International Journal of REmote Sensing*, *28*, 2111–2121.

Wulder, M., Skakun, R., Kurz, W., & White, J. (2004). Estimating time since forest disturbance using segmented Landsat ETM+ imagery. *Remote Sensing of Environment*, *93*, 179–187.

Wulder, M., White, J. C., & Bentz, B. (2004). Detection and mapping of mountain pine beetle red attack: Matching information needs with appropriate remotely sensed data. Bethesda, Maryland: Society of American Foresters.

Wulder, M. A., Dymond, C. C., White, J. C., Leckie, D. G., & Carroll, A. L. (2006). Surveying mountain pine beetle damage of forests: A review of remote sensing Opportunities. *Forest Ecology and Management*, *221*, 27–41.

Wulder, M. A., Skakun, R. S., Dymond, C. C., Kurz, W. A., & White, J. C. (2005). Characterization of the diminishing accuracy in detecting forest insect damage over time. *Canadian Journal of Remote Sensing*, *31*, 421–431.

White, J. C., Coops, N. C., Hilker, T., Wulder, M. A., & Carroll, A. L. (2007). Detecting mountain pine beetle red attack damage with EO-1 hyperion moisture indices. *International Journal of Remote Sensing*, *28*(10), 2111–2121.